American Mineralogist, Volume 71, pages 1384–1392, 1986

Optical properties of single crystals in the order-disorder series low albite–high albite

SHU-CHUN SU,[1] PAUL H. RIBBE, F. DONALD BLOSS
Department of Geological Sciences, Virginia Polytechnic Institute and State University, Blacksburg, Virginia 24061, U.S.A.
JULIAN R. GOLDSMITH
Department of the Geophysical Sciences, University of Chicago, 5734 South Ellis Avenue, Chicago, Illinois 60637, U.S.A.

ABSTRACT

Single crystals were selected from a suite of seven partly to highly disordered albites prepared by heating low albite ($Ab_{99.7}Or_{0.3}An_{0.0}$) from Clear Creek, California, at temperatures of 750 to 1000°C for 6 to 19 d in a piston-cylinder device. Refractive indices (at 589 nm) and extinction angles were found to vary linearly relative to the degree of (Al,Si) order as determined from the reciprocal lattice angles α^* and γ^* measured on X-ray precession photographs. Values for completely ordered low albite (LA) and values extrapolated from LA through our intermediate and high albites to the completely disordered endmember (called analbite, AA) are

End-member	n_α	n_β	n_γ	$2V_X$	$X' \wedge [100]$ on (010)	$X' \wedge [100]$ on (001)	Θ	Ψ	Φ
AA	1.5276	1.5350	1.5363	45.0°	6.2°	9.4°	68.7°	128.5°	99.3°
LA	1.5288	1.5329	1.5394	103.0°	20.8°	3.2°	84.2°	107.2°	88.8°

The easily measured optic axial angle $2V$ varies nonlinearly with (Al,Si) order. It can be used to estimate structural state using the following equations:

$$\Sigma t_1 \equiv (t_1o + t_1m) = 0.353(17) + 1.014(37)\sin^2 V_X,$$

$$\Delta t_1 \equiv (t_1o - t_1m) = -0.353(39) + 2.121(83)\sin^2 V_X,$$

where t_1o and t_1m are the Al contents of the T_1O and T_1m tetrahedral sites, respectively, and $V_X = (2V_X)/2$.

INTRODUCTION

The structural and thermodynamic aspects of (Al,Si) order in albite have received much attention, but few systematic investigations have been conducted on the variation of the optical properties of albites as a function of structural state. Measurements of the optic axial angle $2V$ (Raase and Kern, 1969) and extinction angles (Raase, 1978) on a series of synthetic albites are the only data available for intermediate structural states. The paucity of data is due to the difficulty in obtaining suitable single crystals, and although the optical measurements of previous workers were done on single grains, the structural state was assessed from unit-cell dimensions or the parameter $\Delta 131 \equiv 2\theta(131) - 2\theta(1\bar{3}1)$ determined by X-ray powder methods. However, in this investigation it was possible to carry out both optical measurements and X-ray precession photography on the same single crystal for eight samples of different structural states, produced by a new technique. This has provided the first precise characterization of the optical properties of albite as a function of the reciprocal lattice angles α^* and γ^*, which in turn may be used to establish an estimate of the (Al,Si) order in each optically characterized crystal (see preliminary report by Su et al., 1985).

EXPERIMENTAL PROCEDURES

An iron-free low albite from Clear Creek, California ($Ab_{99.7}Or_{0.3}An_{0.0}$, electron-microprobe analysis by Ian Steele, University of Chicago), was used as the starting material for this study. Cleavage fragments ranging up to approximately 1 mm in size were embedded in reagent-grade Na_2CO_3 and sealed in gold capsules. The carbonate, although supposedly "anhydrous," contains approximately 1% H_2O; no additional water was added. The capsules were run in NaCl pressure cells in piston-cylinder devices at 17–18 kbar. The Na_2CO_3 is adequately plastic so that single crystals large enough for the optical and X-ray work may be readily recovered after the experiment by dissolving the carbonate in 1 *M* HCl. The determination of the equilibrium disorder-temperature relations of albite and the preparation at high pressures of albite with any desired degree of (Al,Si) order ranging from low albite to highly disordered material are described in Goldsmith and Jenkins (1985).

[1] Permanent address: Institute of Geology, Chinese Academy of Sciences, Beijing, People's Republic of China.

0003–004X/86/1112–1384$02.00

Table 1. Heating conditions, reciprocal lattice angles, Al contents of T sites, diffusive order parameter Q_{od}, and configurational entropy S_c of the Clear Creek albites

Sample	T (°C)	P (kbar)	Time (d)	α^* (°)	γ^* (°)	Δt_1	Σt_1	t_1o	t_1m	t_2o	Q_{od}	S_c [J/(mol·K)]
MAB177	1000	17	6	85.87	88.19	0.11	0.59	0.35	0.24	0.21	0.20	18.4
MAB169	780	17	19	85.96	88.52	0.24	0.64	0.44	0.20	0.18	0.38	17.7
MAB176	775	17	19	85.96	88.66	0.30	0.66	0.48	0.18	0.17	0.45	17.2
MAB171	770	17	15	86.14	89.40	0.59	0.80	0.69	0.10	0.10	0.73	13.3
MAB167	760	18	15	86.26	89.99	0.82	0.92	0.87	0.05	0.04	0.90	7.9
MAB172A	750	17	18	86.31	90.04	0.83	0.93	0.88	0.05	0.04	0.90	7.2
MAB151	750	18	12	86.32	90.14	0.87	0.95	0.91	0.04	0.03	0.93	6.0
LA-CC				86.39	90.46	1.00	1.00	1.00	0.00	0.00	1.00	0.0

These albites were prepared by heating at temperatures of 750 to 1000°C for 6–19 d (Table 1), and they cover the range from about 10 to 90% disordered. Of course, modification of structural state by diffusive (Al-Si) exchange is somewhat slower in relatively large crystals than in fine powders, and this is quite possibly related to rates of hydroxyl or hydrogen diffusion in the albite. But in a study of this sort, it is essential that the crystals used be as homogeneous as possible with respect to structural state. The only nondestructive test we have of this is to examine single-crystal X-ray photographs for sharpness of diffraction spots. Although there is some subjectivity in this approach, all of our specimens were selected after examining zero-level precession photographs of each crystal in both the [100] and [001] orientations. Measurements of the α^* and γ^* reciprocal lattice angles from these photographs provided the basis for characterizing the structural states of these crystals (see Table 1).

It should be pointed out that the degree of (Al,Si) order in these relatively large crystals is not necessarily that of the equilibrium configuration at the temperature of the run, because equilibration of structural state requires longer run times than with the powdered specimens studied by Goldsmith and Jenkins (1985). The reaction to jadeite at the surface of the grains is favored in the lower-temperature experiments. The presence of Na_2CO_3 produces a SiO_2-undersaturated environment, and jadeite becomes stable and is formed at pressures well below those of the albite ⇌ jadeite + quartz curve (Holland, 1980). However, satisfactorily homogeneous single crystals of all degrees of order were produced for this study before the cleavage fragments were too badly corroded by the reaction.

From each sample, a single crystal of 200–500 μm in maximum dimension was selected and mounted on a eucentric goniometer head, usually with **b**, the normal to the (010) cleavage face, subparallel to the glass fiber. The goniometer head was attached to a Supper spindle stage mounted on a Leitz ORTHOLUX polarizing microscope, which was equipped with an interference wedge filter to serve as a monochromator and a photomultiplier eyepiece to determine precise extinction positions. The optic axial angle was measured for each crystal at either one peak wavelength, D = 589 nm, or at three different wavelengths, F = 486 nm, D, and C = 656 nm, by determining extinction positions as the dial axis of the spindle stage was rotated through 360° by 10° increments. The extinction data were then processed by the FORTRAN program EXCALIBR (Bloss and Riess, 1973; Bloss, 1981) which calculated, for each wavelength, the optic axial angle and the orientations of the optic axes and the three principal vibration directions. The standard error of estimate of $2V$ as calculated by EXCALIBR are 0.1 to 0.5° for the Clear Creek albites. Their changes with wavelength (dispersion) were quantitatively calculated by DISPER, a subroutine of EXCALIBR.

Once the principal vibration directions X, Y, and Z were located, each could be successively oriented parallel to the vibration direction of the polarizer so that its associated refractive index could be measured without appreciable error from misorientation. Refractive indices were measured with a refined double-variation method on our calibrated system, which is supported by computer programs with related statistical analysis capabilities. These permit the indices of colorless crystals like albites in the refractive-index range of 1.52–1.60 to be measured with unprecedented accuracy and precision. The standard error of estimate of all indices determined in this study is 0.0001 to 0.0002. For each principal refractive index, n_α, n_β, or n_γ, 30 to 70 matches between the refractive index of the immersion oil and that of the crystal were obtained at different temperatures and wavelengths covering the visible range. Using least-squares methods, the data were fit into the linearized Sellmeier dispersion equation (see Bloss, 1981, p. 128),

$$\frac{1}{n^2 - 1} = a_0 + a_1\left(\frac{1}{\lambda^2}\right), \quad (1)$$

where n is the refractive index measured at wavelength λ. The regression coefficients, a_0 and a_1, can be used to calculate the refractive indices at any given wavelength in the visible range.

After the optical data were collected, the goniometer head was transferred to an X-ray precession camera so that $hk0$ and $0kl$ photographs could be taken with Cu or Mo radiation. The locations of X, Y, and Z and of **a***, **b***, and **c***, obtained from the optical and the X-ray studies, were then jointly plotted on a stereonet after proper conversion of the different settings of the two arcs of the goniometer head during the optical and X-ray investigations. Thus, the optical orientation as well as extinction angles on the (001) and (010) planes could be derived.

The reciprocal lattice angles α^* and γ^* were measured directly from the $hk0$ and $0kl$ precession photographs, using a measuring device with a vernier of 0.05°. For each angle, at least 10 readings were taken and then averaged to obtain the final value of the angle measured (Table 1). Estimated errors of measurement of both α^* and γ^* are less than 0.1°.

Results and discussion

Angles α^* and γ^* and the estimation of (Al,Si) distribution

The line relating γ^* to α^* for increasingly disordered Clear Creek albite (Fig. 1, left) differs slightly from that (Fig. 1, right) by which Kroll and Ribbe (1983) joined the endmembers low albite (LA) and analbite (AA). This discrepancy is puzzling, particularly since the line joining LA and AA follows the trend for 43 synthetic albites as variously measured by Wright and Stewart (1968), Raase and Kern (1969), Martin (1970), and Kroll et al. (1980). Crys-

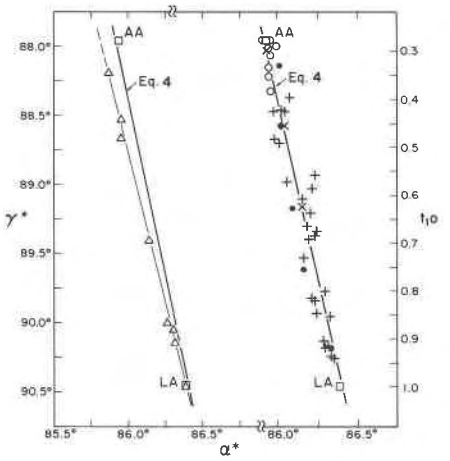

Fig. 1. Reciprocal lattice angles, γ^* versus α^*, for albites. To the left is a plot of data for the Clear Creek albite suite of single crystals (△) with endmembers (□) AA (analbite) and LA (low albite) from Kroll and Ribbe (1983) shown for comparison. To the right is a plot of similar data for synthetic albites: (×) Wright and Stewart (1968), (●) Raase and Kern (1969), (+) Martin (1970), (○) Kroll et al. (1980), and (□) Kroll and Ribbe's AA and LA. The t_1o scale to the right was calculated using Equation 5.

tal-structure analyses of the partially disordered Clear Creek crystals, soon to be undertaken, may supply an explanation. In the meantime, however, one may derive approximate (Al,Si) distributions in these albites using a method first quantified for alkali feldspars in general by Stewart and Ribbe (1969) and expressed in the following regression equation by Kroll and Ribbe (in prep.):

$$\Delta t_1 \equiv (t_1o - t_1m) = \frac{\gamma^* - 44.778 - 0.502\,46\alpha^*}{6.646 - 0.050\,61\alpha^*}, \quad (2)$$

where t_1o and t_1m are the Al contents of the T_1O and T_1m tetrahedral sites. Smith et al. (1986) have recently clarified a nagging uncertainty about the degree of order in low albite by refining its crystal structure at 13 K using neutron diffraction. They demonstrated unequivocally that low albite is completely ordered (within the limit of error) with 0.997(4) Al in T_1O and 1.001(3), 1.002(3), and 1.006(4) Si in T_1m, T_2O, and T_2m, respectively. This result verifies the assumption of complete order implicit in recent structural studies of low albite.

All X-ray and neutron diffraction refinements of feldspar structures have shown that, to a first approximation, $t_2o = t_2m$. It is therefore necessary to determine only one more occupancy value in addition to Δt_1 to obtain a complete estimation of (Al,Si) distribution of all four tetrahedral sites. This is provided by an equation for $(t_1o + t_1m)$ from Kroll and Ribbe (in prep.):

$$\Sigma t_1 \equiv (t_1o + t_1m) = \frac{b - 21.5398 + 53.8405c^*}{2.1567 - 15.8583c^*}. \quad (3)$$

Using the lattice parameters of the 43 synthetic albites and Equations 2 and 3 (see legend of Fig. 1 for references), we calculated t_1o, t_1m, t_2o, and t_2m (= t_2o) and then fit a linear equation for t_1o in terms of γ^*:

$$t_1o = -25.15(15) + 0.2892(17)\gamma^* \qquad [r^2 = 0.999]. \quad (4)$$

At present, Equation 4 is thought to be the best one to estimate t_1o of albites from γ^*. However, because Equation 2 was derived using only the data from the four alkali feldspar endmembers, LA (low albite), AA (analbite), LM (low microcline), and HS (high sanidine) (Kroll and Ribbe, 1983, Table 4), the following equation (similar to Eq. 4 but based solely on the data of Kroll and Ribbe's endmembers LA [$\alpha^* = 86.39°$, $\gamma^* = 90.46°$, $t_1o = 1.0$, $\Delta t_1 = 1.0$] and AA [$\alpha^* = 85.94°$, $\gamma^* = 87.96°$, $t_1o = 0.28$, $\Delta t_1 = 0$]), was used henceforth in our calculations to ensure internal consistency of the estimations:

$$t_1o = -25.05 + 0.2880\gamma^*. \quad (5)$$

If drawn in Figure 1, Equation 5 would be represented by a straight line precisely joining the points labeled LA and AA; it is statistically identical to and nearly coincident with the bold line representing Equation 4.

Using Equations 2 and 5 plus the observed α^* and γ^* values, and assuming $t_2o = t_2m$, we can calculate the (Al,Si) distribution among all four tetrahedral sites as well as the configurational entropy,

$$S_c = -R\Sigma[X_i \ln X_i + (1 - X_i)\ln(1 - X_i)],$$

where R is the gas constant, X_i is mole fraction of Al as calculated above, and the summation is carried out over four tetrahedral sites. See Table 1. The diffusive order parameter Q_{od} used by Salje (1985) can also be calculated, because $Q_{od} = \Delta t_1/\Sigma t_1$. It is evident that all these calculations involving (Al,Si) occupancies, although the best estimates currently available, are strongly model-dependent. Thus caution must be exercised in their use and interpretation.

It should be noted in Table 1 that none of our samples are analbites having both $t_1o = t_1m$ and $t_2o = t_2m$. Thus, we use the term *high albite* (HA) for the most disordered of our series, but use *analbite* (AA) for the hypothetical, completely disordered member obtained by projection to $t_1o = t_1m = t_2o = t_2m = 0.25$.

Refractive indices

The principal refractive indices for light vibrating parallel or most nearly parallel to crystallographic axes **a**, **b**, and **c**—respectively symbolized n_a (= n_α), n_b (= n_γ), and n_c (= n_β) as suggested by Su et al. (1984) and Bloss (1985)—were determined for Fraunhofer lines *F, D,* and *C* (Table 2), but only those for *D* have been plotted versus γ^* and Δt_1 in Figure 2. The resultant trends, linear within the limits of measurement, show that as γ^*, Δt_1, and Σt_1 and thus the degree of (Al,Si) order increase from HA to LA, n_b increases, n_c decreases, and n_a increases. Consequently, as Figure 2 illustrates, the optic sign changes from negative to positive at $(t_1o - t_1m) \cong 0.71$. The relationship between the principal refractive indices and the structural states

can be explained by analogy with the interpretation proposed by Stewart and Ribbe (1969) and Su et al. (1984) for K-rich alkali feldspars. From HA (or AA) to LA, the number of Al atoms encountered in the tetrahedral framework along the **b** axis (Al_b) decreases from 1.5 to 1.0, and the number of Al atoms encountered along the **c** axis (Al_c) increases from 0.75 to 1.0. In fact,

$$Al_b = 2 - \Sigma t_1 \quad \text{and} \quad Al_c = (1 + \Sigma t_1)/2$$

(Su et al., 1984, Fig. 3 and Eqs. 4 and 5). Thus the variations of Al_b and Al_c with (Al,Si) ordering cause the b cell edge to decrease in length by about twice as much as the c cell edge increases. Because the three principal vibration directions X, Z, and Y of the albite indicatrix are subparallel to crystallographic axes **a**, **b**, and **c**, respectively, the variations of the corresponding indices n_a, n_b, and n_c (in that order; Fig. 2), can be accounted for, to a first approximation, by contraction of a and b and by expansion of c from HA to LA. Linear Equations 12–14, relating n_α, n_β, and n_γ at 589 nm to γ^*, Δt_1, and Σt_1 are listed in Table 3, which summarizes the results of a number of regressions performed on the data to obtain either linear or quadratic regression equations of the form

$$y = a_0 + a_1 x \quad \text{or} \quad y = a_0 + a_1 x + a_2 x^2.$$

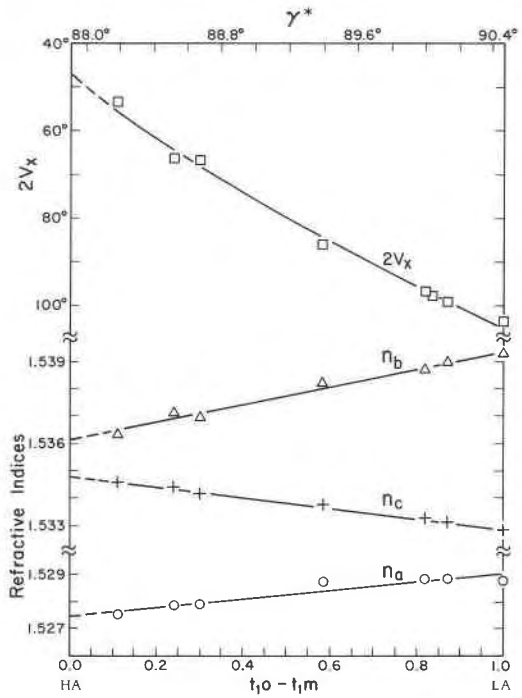

Fig. 2. Refractive indices and $2V_X$ at 589 nm plotted versus Δt_1 and γ^* for Clear Creek albites. The curve for $2V_X$ is calculated from the linear regression Equations 12b, 13b, and 14b in Table 3, relating n_α, n_β, and n_γ to Δt_1.

The dispersions of refractive indices

From the analysis of the refractive-index dispersion data for more than 100 ionic and covalent materials (solids and liquids), Wemple and DiDomenico (1969, 1971) used a single-oscillator description of the frequency-dependent dielectric constant, which equals the square of the refractive index n, to define a "dispersion-energy" parameter E_d. The analytical expression is

$$n^2 - 1 = E_d E_o/(E_o^2 - h^2\omega^2), \qquad (6)$$

where n is the refractive index at frequency ω, E_d is the dispersion energy, E_o is the single oscillatory energy, and h is Planck's constant.

The parameter E_d, a measure of the strength of interband optical transition, is related to the charge distribution within each unit cell and thus is a quantity closely related to chemical bonding. E_d is found to obey the simple empirical relationship

$$E_d = \beta N_c Z_a N_e,$$

where β is a coefficient whose value depends on the nature of the chemical bonding (ionic or covalent), N_c is the coordination number of the cation that is the nearest neighbor to the anion, Z_a is the formal chemical valency of the anion, and N_e is the effective number of valence electrons per anion. Wemple and DiDomenico (1969, 1971) stated that the observed simple dependence on coordination number and chemical valency suggests further that nearest-neighbor atomic-like quantities strongly influence the electronic optical properties of materials.

Table 2. Observed and calculated optic axial angles $2V_x$, extinction angles $X' \wedge [100]$ on (010) and on (001) (in degrees), and refractive indices of the Clear Creek albites

	589 nm (*D*)			486 nm (*F*)				589 nm (*D*)				656 nm (*C*)			
Sample	$2V_X^{obs}$	(010)	(001)	n_α	n_β	n_γ	$2V_X^{calc}$	n_α	n_β	n_γ	$2V_X^{calc}$	n_α	n_β	n_γ	$2V_X^{calc}$
MAB177	53.6	7.8	9.0	1.5333	1.5408	1.5426	52.0	1.5276	1.5346	1.5364	53.6	1.5251	1.5322	1.5340	53.2
MAB169	66.1	9.7	7.5	1.5338	1.5405	1.5434	66.4	1.5279	1.5344	1.5372	66.3	1.5255	1.5321	1.5348	65.0
MAB176	66.7	10.4	7.4	1.5334	1.5402	1.5431	66.0	1.5279	1.5342	1.5370	67.1	1.5257	1.5318	1.5346	68.0
MAB171	85.9	15.5	6.2	1.5346	1.5397	1.5444	87.4	1.5288	1.5338	1.5383	86.7	1.5265	1.5314	1.5360	87.9
MAB167	96.6	17.5	3.8	1.5351	1.5394	1.5449	96.8	1.5289	1.5333	1.5388	96.1	1.5267	1.5310	1.5364	96.2
MAB172A	97.4	19.4	3.8												
MAB151	98.8	18.0	4.6	1.5347	1.5391	1.5451	98.6	1.5289	1.5332	1.5391	98.7	1.5266	1.5308	1.5366	98.9
LA-CC	103.4	21.0	3.3	1.5347	1.5389	1.5455	102.5	1.5288	1.5329	1.5394	102.8	1.5264	1.5305	1.5368	101.9

Table 3. Equations relating α^* to γ^* and refractive indices, extinction angles (degrees), and Euler angles (degrees) at 589 nm to γ^*, Σt_1, and/or Δt_1

Eq. no.	Dep. var.	Ind. var.	a_0	a_1	a_2	r^2	s	Ext. LA $\Sigma t_1 = 1.0$	Ext. AA $\Sigma t_1 = 0.5$
11	α^*	γ^*	65.73(53)	0.2284(59)		0.996	0.0140		
12a	$n_\alpha(n_a)$	γ^*	1.4748(89)	0.00060(10)		0.878	0.0002	1.5291	1.5276
12b	$n_\alpha(n_a)$	Δt_1	1.52754(17)	0.00154(26)		0.877	0.0002	1.5291	1.5275
12c	$n_\alpha(n_a)$	Σt_1	1.52584(43)	0.00323(53)		0.879	0.0002	1.5291	1.5275
13a	$n_\beta(n_c)$	γ^*	1.5992(22)	−0.00073(2)		0.995	0.0001	1.5332	1.5350
13b	$n_\beta(n_c)$	Δt_1	1.53483(4)	−0.00188(6)		0.995	0.0001	1.5330	1.5348
13c	$n_\beta(n_c)$	Σt_1	1.53689(11)	−0.00394(15)		0.993	0.0001	1.5330	1.5350
14a	$n_\gamma(n_b)$	γ^*	1.42280(69)	0.00129(78)		0.982	0.0002	1.5395	1.5363
14b	$n_\gamma(n_b)$	Δt_1	1.53617(13)	0.00330(21)		0.981	0.0002	1.5395	1.5362
14c	$n_\gamma(n_b)$	Σt_1	1.53253(30)	0.00696(38)		0.985	0.0002	1.5395	1.5360
15a	Ext.(010)	γ^*	−492(28)	5.7(3)		0.983	0.7	20.8	6.6
15b	Ext.(010)	Δt_1	6.2(6)	14.6(8)		0.982	0.7	20.8	6.2
15c	Ext.(010)	Σt_1	−9.8(1.3)	30.6(1.6)		0.984	0.7	20.8	5.5
16a	Ext.(001)	γ^*	222(19)	−2.4(2)		0.958	0.5	3.1	9.2
16b	Ext.(001)	Δt_1	9.4(4)	−6.2(5)		0.958	0.5	3.2	9.4
16c	Ext.(001)	Σt_1	16.2(9)	−13.0(1.1)		0.957	0.5	3.2	9.7
17	Θ	Δt_1	68.7(6)	15.5(9)		0.980	0.8	84.2	68.7
18	Ψ	Δt_1	128.5(1.5)	−49.4(7)	28.1(6.0)	0.981	1.1	107.2	128.5
19	Φ	Δt_1	99.3(4)	−10.5(6)		0.981	0.5	88.8	99.3
20	I	Δt_1	43.4(1.3)	−49.5(6.1)	24.1(5.4)	0.990	1.0	18.0	43.4
21	Lα	Δt_1	151.1(3.5)	−32(16)	43(15)	0.873	2.6	162.1	151.1
22	R	Δt_1	31.3(3.8)	33(17)	−48(15)	0.910	2.7	16.3	31.3
23	N	Δt_1	125.9(1.4)	−44.0(6.3)	25.2(5.6)	0.979	1.0	107.1	125.9
24	Kα	Δt_1	155.5(7)	18.9(1.1)		0.982	0.9	174.4	155.5
25	D	Δt_1	−5.5(7)	15.1(3.1)	−12.8(2.8)	0.830	0.5	−3.2	−5.5

Note: Equations derived by least-squares regression methods. The numbers in parentheses are the standard errors of estimate referring to last digit(s). The term a_0 is the intercept, and a_1 and a_2 are coefficients of γ^* (Δt_1 or Σt_1) and Δt_1, respectively. Coefficient of determination r^2, square root of mean square errors s, and extrapolated values for the endmembers LA ($\gamma^* = 90.46°$, $\Delta t_1 = 1.0$, $\Sigma t_1 = 1.0$) and AA ($\gamma^* = 87.96°$, $\Delta t_1 = 0.0$, $\Sigma t_1 = 0.5$) are also listed.

Values of E_d, E_o, and λ_o can be easily calculated from the Sellmeier dispersion constants a_0 and a_1 by using the following equations derived from Equation 6:

$$E_d = \left(\frac{1239.8}{-a_0 a_1}\right)^{1/2}, \quad E_o = \left(\frac{1239.8}{-(a_1/a_0)}\right)^{1/2}, \quad \lambda_o = \left(-\frac{a_1}{a_0}\right)^{1/2}. \qquad (7)$$

We strongly suggest that these quantities be reported in all optical investigations of nonopaque minerals so that a data base of dispersion parameters will be established. Ultimately, new insight may be gained into the optical properties of matter and their relationships to chemical bonding and other features of crystal structures.

The calculations of E_d, E_o, and λ_o of the Clear Creek albites (Eqs. 7 and Table 4) show that these values are very insensitive to the distributions of (Al,Si) among the tetrahedral sites in albites. The grand mean values, i.e., the mean values of all the principal vibration directions, are $E_d = 16.7$ eV, $E_o = 12.7$ eV, and $\lambda_o = 97.7$ nm. These may be compared to the values $E_d = 19.1$ eV, $E_o = 13.0$ eV, and $\lambda_o = 95.3$ nm obtained from optical measurements on an anorthite ($An_{97.5}Ab_{2.4}Or_{0.1}$) from Mt. Somma, Vesuvius, Italy, by S.C.S.

Optic axial angle

It should be emphasized that, because n_j, n_β, and n_γ are linear functions of γ^*, Δt_1, or Σt_1, the optic axial angle $2V_X$ cannot be, since $\sin^2 V_X = (n_\gamma^{-2} - n_\beta^{-2})/(n_\gamma^{-2} - n_\alpha^{-2})$. A predicted $2V_X$ curve is calculated from Equations 12b, 13b, and 14b in Table 3, which relate Δt_1 to n_α, n_β, and n_γ at 589 nm; it is plotted in Figure 2 and fits the observed $2V_X$ data points quite well. In albites the Y-Z plane is very close to the **b**-**c** plane (see inset to Fig. 4). The structural anisotropy within the **b**-**c** plane, which is mainly determined by the (Al,Si) distribution among the four nonequivalent tetrahedral sites, is the least for HA (or AA) and the greatest for LA. This accounts for the smaller difference between n_β and n_γ for HA (or AA) and the greater difference between n_β and n_γ for LA. Accordingly, from HA (AA) to LA, $2V_X$ increases with ordering.

The $2V_X$ values for ordered low albite in the literature include 102.8° (Ramona, California; J. R. Smith, 1958), 103.0° and 102.5° (Tiburon, California; Crawford, 1966; Su, pers. comm.), and 102.9° (Amelia, Virginia; Wolfe, 1976). For heated Amelia albites, Tuttle and Bowen (1950) reported $2V_X$ values of 45–55°, and Laves and Chaisson (1950) reported 40° and 60°; the former measured 45° and the latter 56 ± 3° on synthetic albites. J. R. Smith (1958) determined mean $2V_X$ values of 46.9° on heated Ramona, California, and 45.3° and 46.7° on heated Amelia, Virginia, albite crystals. With one exception, it would appear that 45° is the limiting $2V_X$ value for most highly disordered albite. We cannot be sure which samples were HA or which AA, although if any are *completely* disordered, they must be analbites.

Table 4. Dispersion energy E_d (eV), single-oscillator energy E_o (eV), and single-oscillator wavelength λ_o (nm) associated with n_α, n_β, and n_γ of the Clear Creek albites

	n_α			n_β			n_γ		
Sample	E_d	E_o	λ_o	E_d	E_o	λ_o	E_d	E_o	λ_o
MAB177	16.7	12.9	96.4	16.5	12.5	99.1	16.6	12.6	98.6
MAB169	16.6	12.8	97.2	16.9	12.8	96.9	16.7	12.6	98.6
MAB176	17.1	13.2	94.3	16.6	12.6	98.2	16.6	12.5	98.9
MAB171	16.8	12.9	96.3	16.8	12.7	97.3	16.8	12.7	97.3
MAB167	16.4	12.6	98.1	16.6	12.7	97.9	16.9	12.7	97.4
MAB151	16.6	12.8	97.0	16.7	12.7	98.0	16.7	12.6	98.7
LA-CC	16.4	12.6	98.2	16.7	12.7	97.3	16.6	12.5	99.1

These optic axial angles are close to values we obtained: 103.4° (observed) and 102.8° (calculated from refractive indices) for the Clear Creek, California, low albite (Table 2) and an extrapolated value of 45° for the most disordered albite. The latter was arrived at by assuming $\Sigma t_1 = 0.5$ in Equation 8, as given below.

For K-rich feldspars, Su et al. (1984) observed that Σt_1, the Al content of the T_1 sites, was linearly related to $\sin^2 V_X$. Their Equations 13a and 13b permitted Σt_1 to be closely estimated from the optical axial angle $2V_X$ of a K-rich feldspar, a quantity much more easily determined than the lattice parameters **b** and **c***. Similar regression equations permit Σt_1, Δt_1, and Q_{od} to be estimated for these albites provided $2V_X$ is known:

$$\Sigma t_1 = +0.353(17) + 1.014(37)\sin^2 V_X \quad (8)$$
$$[r^2 = 0.992,\ s = 0.02],$$
$$\Delta t_1 = -0.353(39) + 2.121(83)\sin^2 V_X \quad (9)$$
$$[r^2 = 0.991,\ s = 0.03],$$
$$Q_{od} = -0.169(27) + 1.910(57)\sin^2 V_X \quad (10)$$
$$[r^2 = 0.995,\ s = 0.02].$$

For these equations the numbers in parentheses that follow each number represent the standard error of that number in terms of its last units cited. Thus 0.353(17) indicates a standard error of 0.017 for 0.353; r^2 is the coefficient of determination, and s is the square root of the mean square errors. The high r^2 values and small s values for regression Equations 8–10 indicate that $2V_X$, an easily measured quantity, may also serve to estimate the (Al,Si) distributions over the tetrahedral sites of albites. Indeed, the precision is comparable to that obtainable by use of lattice parameters.

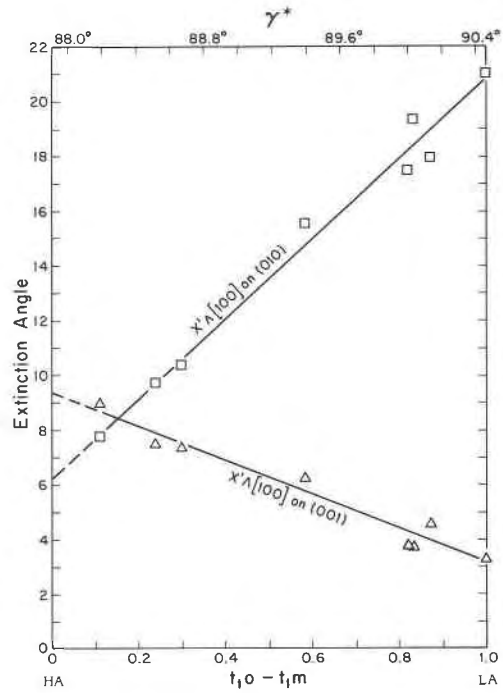

Fig. 3. Extinction angles $X' \wedge [100]$ on (001) and $X' \wedge [100]$ on (010) at 589 nm versus γ^* and Δt_1 for Clear Creek albites. The lines represent Equations 15a, 15b, 16a, and 16b in Table 3.

Subject to the limitations inherent in the methods for estimating (Al,Si) distributions from lattice constants and the restricted experimental data in this study, Equations 8, 9, and 10 imply that both ($t_1o + t_1m$) and ($t_1o - t_1m$)

Table 5. Spherical coordinates of two optic axes A_1 and A_2 and principal vibration directions X, Y, and Z (degrees) of Clear Creek albites and extrapolated endmembers, analbite AA(EXT) and low albite LA(EXT)

	A_1		A_2		X		Y		Z	
Sample	φ	ρ	φ	ρ	φ	ρ	φ	ρ	φ	ρ
HA(BPW)	248.5	66.0	298.3	82.1	274.5	72.5	45.0	25.9	178.5	71.5
AA(EXT)	258.1	56.1	296.8	83.5	279.3	68.7	33.8	43.2	175.7	54.6
MAB177	252.3	57.6	300.3	86.8	278.4	70.7	34.3	38.8	175.7	57.8
MAB169	242.4	61.0	305.5	88.8	276.3	72.5	37.4	31.5	177.8	64.8
MAB176	241.5	61.6	306.3	89.6	276.2	73.1	36.9	30.7	178.1	65.1
MAB171	229.8	67.6	133.3	85.3	273.5	78.2	32.3	23.4	179.1	70.1
MAB167	221.5	71.2	136.3	83.7	270.4	80.8	28.0	19.3	177.6	73.2
MAB172A	221.1	73.0	136.6	82.8	270.1	82.7	23.4	17.8	177.9	73.8
MAB151	220.8	71.2	138.4	83.1	271.1	81.0	28.2	19.2	178.4	73.2
LA-CC	217.2	73.5	138.3	79.9	268.6	85.0	14.6	17.8	177.1	72.9
LA(EXT)	217.3	73.0	138.1	80.4	268.8	84.2	16.9	18.1	177.0	72.9
LA(BPW)	218.2	73.4	138.1	81.2	269.2	84.0	18.6	17.5	177.4	73.6

Note: Data for the endmembers were derived from the respective extrapolated Euler angles Θ, Ψ, and Φ listed in Table 3, at 589 nm. Projection plane is perpendicular to +**c**, and +**b*** is toward the E (east) direction as in Fig. 4. LA(BPW) and HA(BPW) refer to endmember data of Burri et al. (1967, p. 271), which are listed here for comparison. Spherical coordinate angle φ is measured clockwise starting from +**b***.

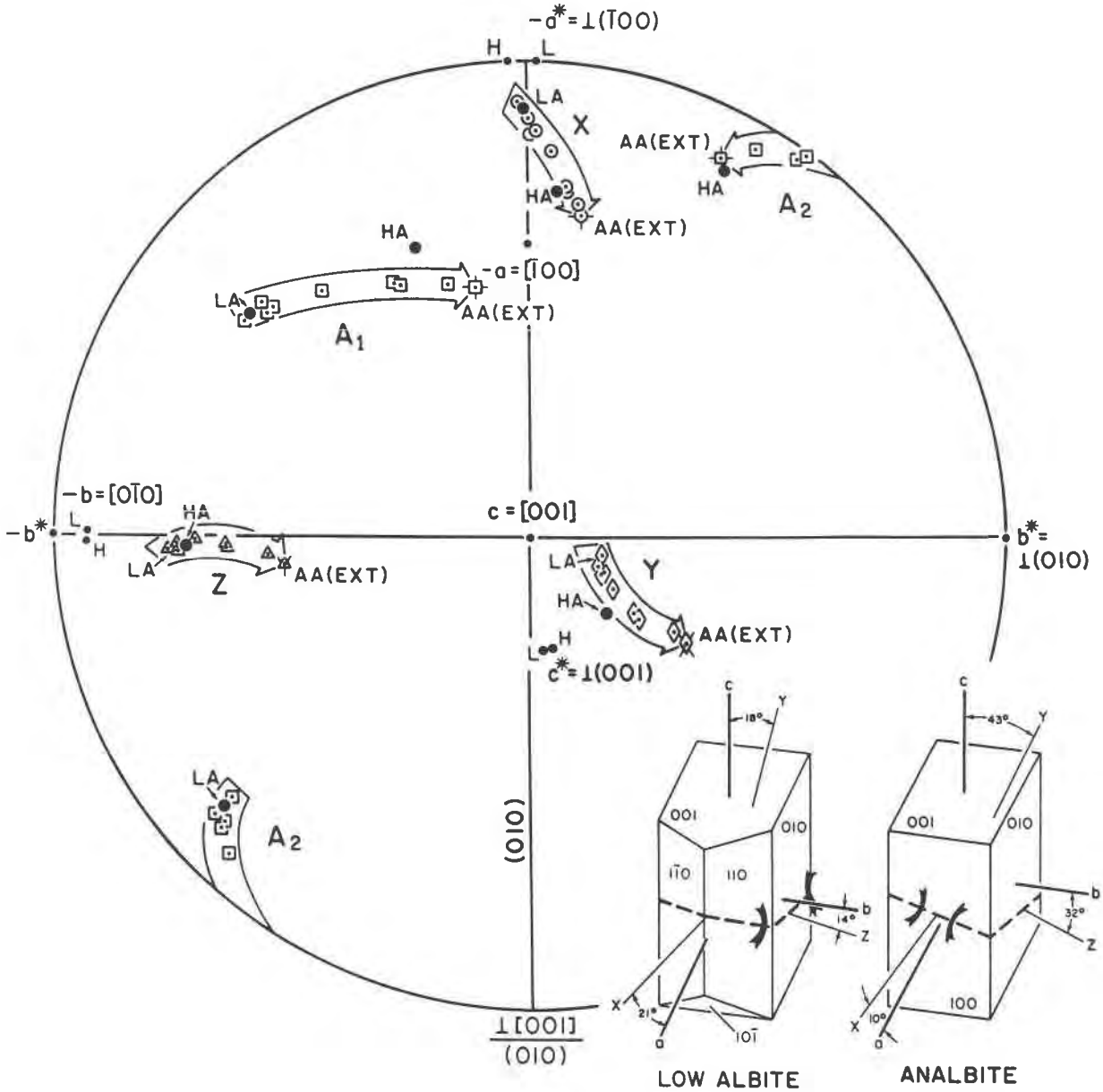

Fig. 4. Optical orientations of the Clear Creek albites and the extrapolated AA(EXT) endmember analbite at 589 nm. Points for AA(EXT) are indicated by branching lines. The projection plane is perpendicular to +**c** with +**b*** pointing E (East). The large dots labeled LA and HA are the endmembers low albite and high albite of Burri et al. (1967). [The symbols of LA from Burri et al. (1967) for *Y* and *Z* fall right on the Clear Creek albite points and are thus omitted from this diagram for clarity.] The direct and reciprocal crystallographic axes of the Clear Creek albites are represented by small dots. The labels L and H correspond to the samples LA-CC and MAB177, respectively (Table 5). The hollow arrows show the migration trends from low albite to analbite. The optical orientation diagrams of analbite and low albite are based on the Euler angle data of the extrapolated endmembers AA(EXT) and LA(EXT), respectively, as listed in Table 3.

as well as their quotient of $(t_1o - t_1m)/(t_1o + t_1m)$ can be determined by the single parameter V_X. In other words, they imply that for any value of Σt_1, there is only one value of Δt_1. Whether this is merely an empirical relationship or the result of one-step ordering remains to be investigated in future structural studies of these crystals.

Extinction angles $X' \wedge [100]$ on (010) and $X' \wedge [100]$ on (001)

Extinction angles were calculated by combining data on the orientation of the optical indicatrix, as obtained by spindle-stage techniques, with data on the crystallographic axis orientation as obtained by X-ray precession photog-

Table 6. Euler angles I, II, and III (Burri et al., 1967) at 589 nm and spherical coordinates φ and ρ (degrees) of crystallographic axes $-\mathbf{a}$, $-\mathbf{b}$, $+\mathbf{a}^*$, and $+\mathbf{c}^*$ of the Clear Creek albites and extrapolated endmembers analbite AA(EXT) and low albite LA(EXT)

	I			II			III			$-a$		$-b$		a^*		c^*	
Sample	Θ	Ψ	Φ	I	$L\alpha$	R	N	$K\alpha$	D	φ	ρ	φ	ρ	φ	ρ	φ	ρ
AA(EXT)	68.7	128.5	99.3	43.4	151.1	31.3	125.9	155.5	−5.5	270.0	63.5	178.5	86.6	88.2	90.0	79.0	27.2
MAB177	70.7	124.3	98.4	38.8	148.1	34.3	122.2	157.0	−4.3	270.0	63.5	178.2	86.3	88.2	90.0	80.8	26.7
MAB169	72.5	116.5	96.3	31.5	144.7	37.4	115.2	160.5	−2.2	270.0	63.5	178.5	86.2	88.5	90.0	81.0	26.7
MAB176	73.1	116.1	96.2	30.7	145.4	36.9	114.9	161.3	−1.9	270.0	63.6	178.7	86.2	88.7	90.0	81.0	26.7
MAB171	78.2	110.3	93.5	23.4	149.0	32.3	109.9	167.5	−0.9	270.0	63.5	179.4	86.0	89.4	90.0	81.4	26.8
MAB167	80.8	107.0	90.4	19.3	151.0	28.0	106.8	170.4	−2.4	270.0	63.4	179.8	85.9	89.8	90.0	81.7	26.8
MAB172A	82.7	106.3	90.1	17.8	155.6	23.4	106.2	172.4	−2.1	270.0	63.4	180.0	85.9	90.0	90.0	81.8	26.8
MAB151	81.0	107.0	91.1	19.2	151.6	28.2	106.8	170.6	−1.6	270.0	63.4	179.9	85.8	89.9	90.0	81.8	26.8
LA-CC	84.9	107.1	88.6	17.8	163.3	14.6	107.1	174.7	−2.9	270.0	63.4	180.5	85.7	90.5	90.0	82.0	26.8
LA(EXT)	84.2	107.2	88.8	18.0	162.1	16.3	107.1	174.4	−3.2	270.0	63.4	180.4	86.3	90.5	90.0	82.0	26.8

Note: Projection plane is perpendicular to $+\mathbf{c}$, and $+\mathbf{b}^*$ is toward the E (east) direction as in Fig. 4. Spherical coordinate angle φ is measured clockwise starting from $+\mathbf{b}^*$.

raphy on the same crystal (see Table 2 and Fig. 3). Because we have not yet measured $2\theta(131) - 2\theta(1\bar{3}1)$ for this suite of albites, it is not possible to compare the results of this study directly with the extinction angles of the suite of synthetic intermediate albites studied by Raase (1978).

Both extinction angles show linear relationships with Δt_1, Σt_1, and γ^* (Eqs. 15a, 15b, 15c, 16a, 16b, and 16c in Table 3). The extrapolated values are 6.2° on (010) and 9.4° on (001) for AA (with $\Sigma t_1 = 0.5$) and 20.8° on (010) and 3.2° on (001) for LA. Raase's extrapolated values are 7.7°, 8.1° and 19.9°, 2.8°, respectively. In Figure 3 the variation of $X' \wedge [100]$ on (010) with order-disorder is greater than that of $X' \wedge [100]$ on (001) because the migration trend for X from HA to LA is subparallel to (010) and nearly perpendicular to (001) (cf. Fig. 4).

Optical orientation

The universal stage was once the major tool for determining optical orientations of feldspars. Because the crystallographic directions were derived indirectly from twinning (twin planes, composition planes, and twin axes) or cleavages, the results were less precise (and less accurate) than those obtained by spindle-stage techniques. Spindle-stage techniques are now capable of locating an optical direction to within a few tenths of a degree and can be used with the X-ray precession method, which is in turn capable of locating both direct and reciprocal crystallographic axes to within 0.1°.

As the Clear Creek albite is increasingly disordered, its three principal vibration axes X, Y, and Z and its two optic axes A_1 and A_2 for the wavelength 589 nm change orientation relative to the crystallographic directions **c** and **b*** (large hollow arrows, Fig. 4; numerical data are listed in Table 5). The extrapolated analbite AA(EXT) plotted in Figure 4 as well as the accompanied optical orientation diagram of analbite was based on the Euler angles I (Θ, Ψ, and Φ) extrapolated to $\Delta t_1 = 0.5$ from Equations 17, 18, and 19 as listed in Table 3. A similar plot of the Burri et al. (1967, Plate V) data for low albite (labeled LA in Fig. 4) conforms to that for the natural Clear Creek albite. In contrast, their data points for high albite (HA) appear discrepant relative to the extrapolated analbite AA(EXT) endmember for A_1, Y, and particularly for Z. For Z the discrepancy approximates 17°, which seems beyond errors of measurement.

The Y-Z planes of albites of differing structural states are all nearly parallel to the **b**-**c** or (100) plane (inset in Fig. 4). Consequently, it is not surprising that, as disordering changes the (Al,Si) distribution among the tetrahedral sites (and thus the relative dimensions along **b** and **c**), the concomitant changes in the values of n_b ($= n_\gamma$) and n_c ($= n_\beta$) will be accompanied by changes in the orientation of Z and Y. Quantitative data for the changes in optic orientation caused by increasing order in the Clear Creek albite are summarized in Tables 5 and 6.

Note that in Table 3, Euler angles Θ, Φ, and K_a, as defined by Burri et al. (1967), appear linearly related to Δt_1 whereas angles Ψ, L_a, I, R, N, and D (Burri et al., 1967) bear a quadratic relationship to Δt_1.

Acknowledgments

This work was supported in part by National Science Foundation Grants EAR-83-08308 to F.D.B. and P.H.R. and EAR-83-05904 to J.R.G. S.C.S. gratefully acknowledges financial support from N.S.F. and a Cunningham Fellowship awarded by Virginia Polytechnic Institute and State University. We are grateful to R. C. Newton for the albite sample, to Ian Steele for the microprobe analysis, and to H. Wondratschek of Karlsruhe and H. Kroll of Münster, and especially to D. B. Stewart of the U.S. Geological Survey, Reston, Virginia, for comments and constructive criticism.

References

Bloss, F.D. (1981) The spindle stage: Principles and practice. Cambridge University Press, Cambridge, England, 340 p.

——— (1985) Labelling refractive index curves for mineral series. American Mineralogist, 70, 428–432.

Bloss, F.D., and Riess, D. (1973) Computer determination of $2V$ and indicatrix orientation from extinction data. American Mineralogist, 58, 1052–1061.

Burri, C., Parker, R.L., and Wenk, E. (1967) Die optische Orientierung der Plagioklase—Unterlagen und Diagramme zur

Plagioklase-bestimmung nach der Drehtische-methode. Birkhäuser, Basel und Stuttgart, 334 p.

Crawford, M.L. (1966) Composition of plagioclases and associated minerals in some schists from Vermont, U.S.A., and South Westland, New Zealand, with inferences about the peristerite solvus. Contributions to Mineralogy and Petrology, 13, 269–294.

Goldsmith, J.R., and Jenkins, D.M. (1985) The high-low albite relations revealed by reversal of degree of order at high pressures. American Mineralogist, 70, 911–923.

Holland, T.J.B. (1980) The reaction albite = jadeite + quartz determined experimentally in the range 600–1200°C. American Mineralogist, 65, 129–134.

Kroll, H., and Ribbe, P.H. (1983) Lattice parameters, composition and Al,Si order in alkali feldspars. Mineralogical Society of America Reviews in Mineralogy, 2, 2nd edition, 57–100.

Kroll, H., Bambauer, H.-U., and Schirmer, U. (1980) The high albite–monalbite and analbite-monalbite transitions. American Mineralogist, 65, 1192–1211.

Laves, F., and Chaisson, U. (1950) An X-ray investigation of the "high"–"low" albite relations. Journal of Geology, 58, 584–592.

Martin, R.F. (1970) Cell parameters and infra-red absorption of synthetic high to low albites. Contributions to Mineralogy and Petrology, 26, 62–74.

Raase, P. (1978) Extinction angles of synthetic intermediate albites. American Mineralogist, 63, 466–469.

Raase, P., and Kern, H. (1969) Über die synthese von Albiten bei Temperaturen von 250 bis 700°C. Contributions to Mineralogy and Petrology, 21, 225–237.

Salje, E. (1985) Thermodynamics of sodium feldspar I. Order parameter treatment and strain induced coupling effects. Physics and Chemistry of Minerals, 12, 93–98.

Smith, J.R. (1958) Optical properties of heated plagioclases. American Mineralogist, 43, 1179–1194.

Smith, J.V., Artioli, G., and Kvick, Å. (1986) Low albite, $NaAlSi_3O_8$: Neutron diffraction study of crystal structure at 13 K. American Mineralogist, 71, 727–733.

Stewart, D.B., and Ribbe, P.H. (1969) Structural explanation for variations in cell parameters of alkali feldspar with Al/Si ordering. American Journal of Science, 267-A, 444–462.

Su, S.C., Bloss, F.D., Ribbe, P.H., and Stewart, D.B. (1984) Optic axial angle, a precise measure of Al,Si ordering in T_1 tetrahedral sites of K-rich alkali feldspars. American Mineralogist, 69, 440–448.

Su, S.C., Ribbe, P.H., Bloss, F.D., and Goldsmith, J.R. (1985) Structural states and properties of a low-high albite series of single crystals. Geological Society of America Abstracts with Programs, 17, 729.

Tuttle, O.F., and Bowen, N.L. (1950) High-temperature albite and contiguous feldspars. Journal of Geology, 58, 572–583.

Wemple, S.H., and DiDomenico, M., Jr. (1969) Optical dispersion and the structure of solids. Physical Review Letters, 23, 1156–1160.

——— (1971) Behavior of the electronic dielectric constant in covalent and ionic materials. Physical Review B, 3, 1338–1351.

Wolfe, H.E. (1976) Optical and X-ray study of the low plagioclase. M.S. thesis, Virginia Polytechnic Institute and State University, Blacksburg, Virginia.

Wright, T.L., and Stewart, D.B. (1968) X-ray and optical study of alkali feldspars: I. Determination of compositions and structural state from refined unit-cell parameters and $2V$. American Mineralogist, 53, 38–87.

Manuscript received November 25, 1985
Manuscript accepted August 6, 1986